Journal of Power Sources 205 (2012) 71–79

Contents lists available at SciVerse ScienceDirect

Journal of Power Sources

journal homepage: www.elsevier.com/locate/jpowsour

Electrocatalysis of Ni-promoted Cd coated graphite toward methanol oxidation in alkaline medium

Ali Döner[a], Esra Telli[b], Gülfeza Kardaş[a,*]

[a] Çukurova University, Science and Letters Faculty, Chemistry Department, 01330 Adana, Turkey
[b] Osmaniye Korkut Ata University, Vocational School of Bahçe, Technical Programs Department, Chemical Technology Programme, 80500 Bahçe Osmaniye, Turkey

ARTICLE INFO

Article history:
Received 18 October 2011
Received in revised form
13 December 2011
Accepted 1 January 2012
Available online 9 January 2012

Keywords:
Methanol oxidation
Catalysis
Nickel
Cadmium
Graphite

ABSTRACT

The nickel–cadmium (Ni-promoted Cd) catalyst for using direct methanol fuel cell (DMFC) applications is electrochemically deposited on a graphite substrate. The activity of methanol oxidation is assessed by recording cyclic voltammetry, electrochemical impedance spectroscopy (EIS) and chronoamperometry (CA) techniques. The surface morphologies and chemical compositions of catalysts are determined by scanning electron microscopy (SEM), energy dispersive X-ray spectroscopy (EDX) and X-ray florescence spectroscopy (XRF). Mean roughness of catalysts is measured by atomic force microscopy (AFM). Kinetic parameters of oxidation such as the anodic electron transfer coefficient (α_a), cathodic electron transfer coefficient (α_c) and charge transfer rate constant (k_s) are calculated. The effect of methanol concentration and temperature on methanol oxidation is also investigated. The electrochemical measurements show that the addition of Cd to single coating enhances the electrocatalytic properties for methanol oxidation and Ni-promoted Cd/C has the best catalytic activity and stability.

1. Introduction

Direct methanol fuel cell (DMFC) is a promising power source for portable electronic applications due to its low operating temperature, easy transportation and fuel storage, high-energy efficiency, low exhaustion and fast start-up [1]. A lot of projects have been made in the development of DMFCs [2–4]. However, their performance is still limited by the poor kinetics of the anode reaction [5,6] and the crossover of methanol from the anode to the cathode side through the proton exchange membrane [7,8]. Pt is still the most satisfactory electrode material in DMFCs both for its activity and stability, while few materials have achieved comparable performance to Pt. Unfortunately, Pt is easily poisoned by CO_{ad}, which is an intermediate of the methanol oxidation reaction (MOR) [9,10]. The CO_{ad} poisoning could be alleviated by alloying Pt with other metals like Ru [11,12] or Ni [13,14]. Ni has commonly been used as an electrocatalyst for both anodic and cathodic reactions in organic synthesis and water electrolysis [15–18]. One of the very important uses of nickel as a catalyst is for the oxidation of alcohols. Several studies of the electro-oxidation of alcohols on Ni have been reported [19,20].

Carbon based materials are commonly used as DMFC catalyst support materials. However, these conventional carbon materials have been investigated for a long time, and substantial information has already been accumulated. In addition, the choice of suitable carbon based materials for the catalysts is also an important factor that can significantly affect the performances of supported catalysts owing to interactions, which modify the catalytic activities of metal catalysts and carbon support materials [21]. Because of a good electrochemical stability, unique structures, low cost, low overpotential, high electronic and thermal conductivities and a high specific surface area, graphite (C) as a catalyst support to improve the catalyst utilization and electroactivity in fuel cells have been extensively studied [22]. A combination of a large surface area with an enhanced catalytic activity and low overpotential enable co-deposits of transition metals and oxides on the graphite substrate.

The aim of present study is preparation of catalyst as an effective anode material for DMFC applications. For this purpose, electrochemical measurements are used to analyze the methanol oxidation on the Ni-promoted Cd/C catalyst.

2. Experimental

The graphite substrate was used as a catalyst support. The graphite rod was coated with polyester block except only a base side of substrate, which was left to contact with the electrolyte and electrical conductivity was provided by a copper wire. Exposed area of substrate is 0.283 cm^2. The substrate surface was polished with emery paper (320–1000 grain size), then washed with distilled water, thoroughly degreased with acetone, followed by

* Corresponding author. Tel.: +90 322 338 6081x16; fax: +90 322 338 6070.
E-mail address: gulfeza@cu.edu.tr (G. Kardaş).

0378-7753/$ – see front matter © 2012 Elsevier B.V. All rights reserved.
doi:10.1016/j.jpowsour.2012.01.020

washing with distilled water again and immersed in the bath solution. The electrodeposition was performed galvanostatically using a Potentiostate-galvanostate instrument (Princeton Applied Research Model 362) with a three-electrode configuration. A nickel sheet was used as counter electrode, and Ag/AgCl electrode was used as the reference electrode. The metal deposition was carried out at room temperature. During metal deposition, the bath solutions were continuously stirred using a magnetic stirrer.

(a) *Preparation of Ni/C*: The catalyst was prepared using a nickel bath solution. The bath composition was 30% $NiSO_4{\cdot}6H_2O$, 1.00% $NiCl_2{\cdot}6H_2O$, 1.25% H_3BO_3 (wt%). A constant current density of 100 mA cm^{-2} was applied to the electrolysis system for 900 s. After deposition, the catalyst was rinsed with distilled water in order to remove residues of bath chemicals and unattached particles.

(b) *Preparation of Ni-promoted Cd/C*: $CdCl_2$ and $CdSO_4$ salts were added to the nickel bath. The bath composition was 0.274% $CdSO_4{\cdot}8/3H_2O$, 0.00787% $CdCl_2$ (wt%). The bath mole ratios of Ni^{2+} and Cd^{2+} are 10:0.1. Prepared catalyst is named as Ni-promoted Cd/C. The amount of Cd was kept very low in the binary catalyst.

Constant current density of 80 mA cm^{-2} was applied to the electrolysis system for 900 s during the electrodeposition. The electrochemical measurements were carried out using a CHI 604 A.C. Electrochemical Analyzer (Serial Number 64721A) under computer control. A double-wall one-compartment cell with a three-electrode configuration was used. A platinum sheet (with 2 cm^2 surface area) and Ag/AgCl electrode was used as the auxiliary and the reference electrodes, respectively. All potential values were referred to this reference electrode. Cyclic voltammograms were recorded at different scan rates, concentrations of methanol and temperatures. Electrochemical impedance spectroscopy (EIS) and chronoamperometry (CA) measurements were performed at a constant potential. The EIS experiments were conducted in the frequency range of 100 kHz to 0.003 Hz at 0.5 V. The amplitude was 0.005 V. The electrochemical tests were carried out in 1.00 M CH_3OH + 1.00 M KOH solution. The solution temperature was

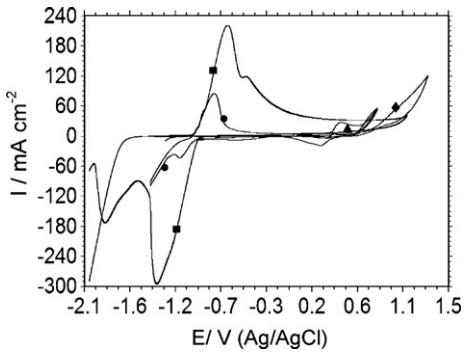

Fig. 1. Cyclic voltammograms of C (♦), Cd/C (■), Ni/C (▲) and Ni-promoted Cd/C (●) in 1.00 M KOH at 25 °C (scan rate ν: 100 mV s^{-1}).

thermostatically controlled at different temperatures by the Nuve BS 302 type thermostat. All the test solutions were prepared from analytical grade chemical reagents in distilled water without further purification. Newly prepared catalysts as well as the test solutions were used for each experiment. All experiments were repeated at least three times.

The chemical composition of catalyst was determined by energy dispersive X-ray (EDX) and X-ray florescence (XRF) analysis. The scanning electron microscopy (SEM) images were taken using a Carl Zeiss Leo 440 SEM instrument at high vacuum and 10 kV EHT. Mean roughness of catalysts is measured by atomic force microscopy (AFM).

3. Results and discussion

3.1. Characterization

Cyclic voltammetry (CV) is an electrochemical technique suitable for the electrochemical characterization of the prepared catalysts [23]. Fig. 1 shows the CVs of C, Cd/C, Ni/C and Ni-promoted Cd/C in 1.00 M KOH solution at 298 K between the hydrogen and oxygen evolution potential range. In Fig. 1, it is seen the process of carbonization on the graphite surface in the alkaline media. When

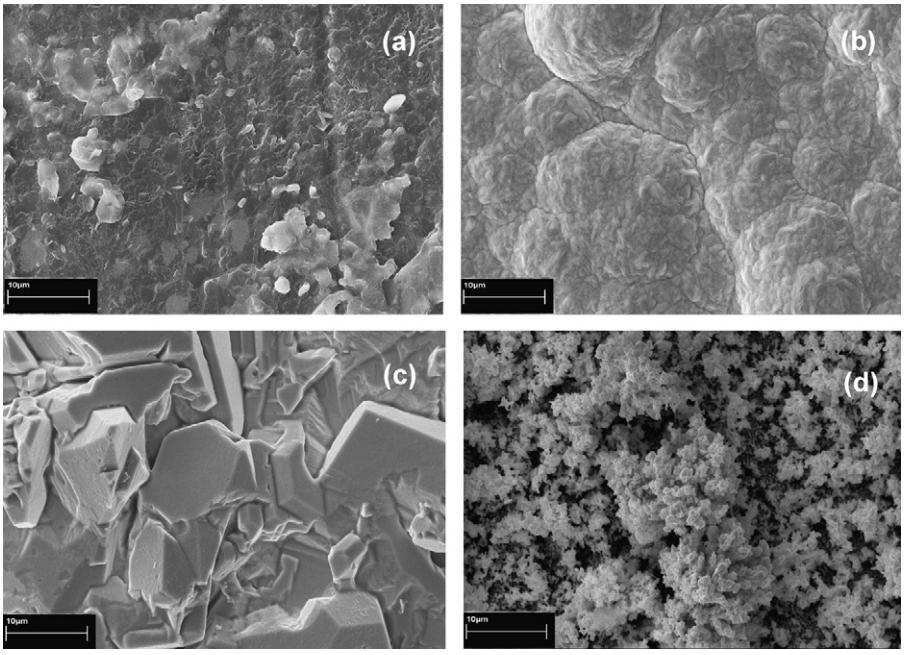

Fig. 2. SEM images of graphite (a) and Ni (b), Cd (c) and Ni-promoted Cd (d) coated graphite electrodes (mag: 5.00k×).

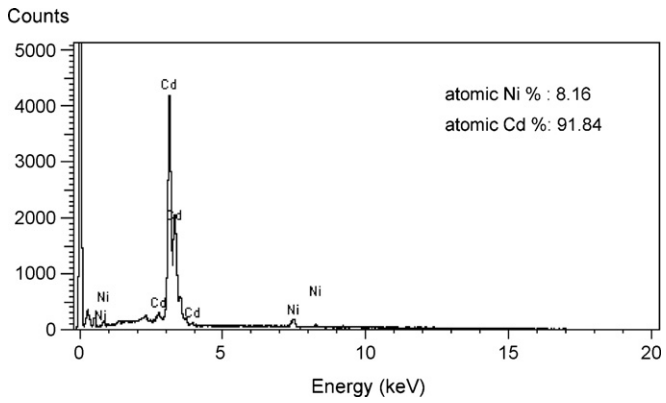

Fig. 3. EDX spectrum obtained from the surfaces of Ni-promoted Cd/C layer.

the graphite surface was coated with the cadmium, the CV of the graphite was changed. Three anodic peaks and four cathodic peaks can be seen. The narrow and large peaks at −0.94 and −0.69 V correspond to formation of soluble cadmium species, as well as solid $Cd(OH)_2$ and CdO [24]. The second anodic peak is due to changes in the anodic layer or to further oxidation of the underlying metal. This peak depends on the scan rate, suggesting that the process is time dependent. The reduction peaks at −1.22 and −1.39 V can involve the reduction of $Cd(OH)_2$ as well as CdO. The occurrence of several cathodic peaks has been explained by the reduction of $Cd(OH)_2$ with different water contents [25,26]. In Fig. 1, the peak at −0.70 V corresponds to Ni/Ni^{2+} oxidation [27,28], the transformation of α-$Ni(OH)_2$ to β-$Ni(OH)_2$ takes place between the potential ranges of −0.57 to 0.32 V [29]. The peak centered at 0.34 V corresponds to the Ni^{2+}/Ni^{3+} transition [20,29,30]. The cathodic peak at 0.30 V corresponds to the Ni^{3+}/Ni^{2+} reduction. In Fig. 1, the CVs of the Ni-promoted Cd/C catalyst shows both the behaviors of Ni and Cd. Anodic and cathodic peak intensity changes by changing the composition of Ni and Cd in the catalyst.

The surface SEM images of graphite (C), Ni/C and Cd/C and Ni-promoted Cd/C are shown in Fig. 2. As it is seen in Fig. 2a, graphite surface consists of some micro sheets. In Fig. 2b and c, the morphology of graphite surface changed significantly when the surface coated with Ni or Cd (Fig. 2b and c). The surface is fully covered by Ni in Fig. 2b or Cd in Fig. 2c. In Fig. 2b nodular structures were distributed on the Ni surface. As seen in Fig. 2c, Cd coating has significantly different crystalline structures than Ni. SEM image and EDX spectra of Ni-promoted Cd/C catalyst are given in Figs. 2d and 3, respectively. As it can be seen from Fig. 2d, when Ni and Cd co-deposited on graphite surface, the surface morphology changed.

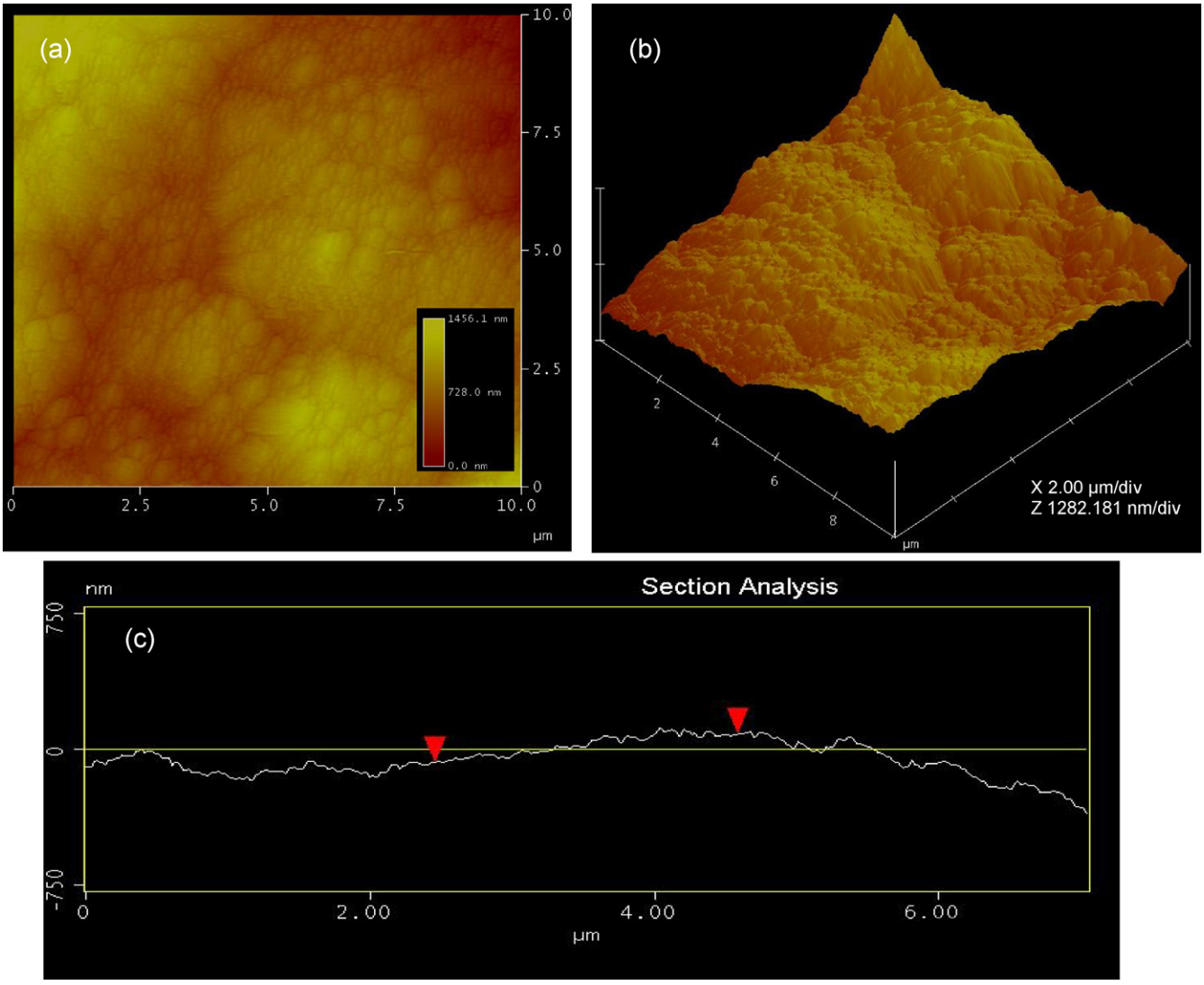

Fig. 4. 2D (a), 3D (b) AFM images, and sectional analysis (c) of Ni/C catalyst.

Catalyst particles like granules were distributed on the surface. The deposit presents a highly porous structure. Moreover, the porosity of surface more and more improved. In the EDX spectrum of Ni-promoted Cd/C catalyst surface, both peaks of Ni and Cd were shown. The related percentage metal ratios are given in the same figures as the inset. The percentage amount of Cd is higher than the percentage amount of Ni. This is related to the reduction rate of Cd^{2+}. Upon the entire surface of Ni-promoted Cd/C, the metal ratios are also measured by XRF. Amount of metal ratios was given as wt%. The related metal ratios are 7.04% Ni and 92.95% Cd. These data are in good agreement with results of EDX. AFM is a powerful technique to investigative the surface morphology at nano- to micro-scale and has become a new choice to study the surface morphology of the coatings. The two (2D) and three-dimensional (3D) AFM images as well as a section analysis of Ni-promoted Cd and Ni/C surfaces are given in Figs. 4 and 5. As it is shown in Fig. 5, the surface of Ni-promoted Cd/C catalyst has a considerably porous structure. By comparing Figs. 4 and 5 and Fig. 2, there is a very good agreement between AFM and SEM images. Mean roughness of Ni/C and Ni-promoted Cd/C catalysts is measured as 142.82 and 486.51 nm, respectively.

3.2. Electrooxidation of methanol on Ni-promoted Cd/C electrocatalyst

Fig. 6 displays the cyclic voltammograms recorded for the oxidation of methanol at a scan rate of 100 mV s^{-1} for C, Ni/C, Cd/C and Ni-promoted Cd/C. As it can be seen from Fig. 6, no current peak of methanol oxidation is observed, indicating that the C and Cd/C have no obvious electrocatalytic activity for methanol oxidation. It is clear from Fig. 6 that two well-defined anodic peaks and one cathodic peak were observed in the forward and backward scans, for the Ni/C and Ni-promoted Cd/C catalysts. Methanol oxidation currents (I_p) during the forward scan were determined as 106.6 and 230.4 mA cm^{-2} for Ni/C and Ni-promoted Cd/C, respectively, from the corresponding CVs. The results obtained showed that the methanol oxidation current increased for Ni-promoted Cd/C catalyst with respect to Ni/C. However, the highest methanol oxidation current was obtained on Ni-promoted Cd/C catalyst. These data suggest that the surface porosity and enhancement of the surface area are not negligible for the Ni-promoted Cd/C catalyst [31]. Synergistic effect between Ni and Cd may also affect the methanol oxidation. Because the Cd is incorporated into the surface Ni layer

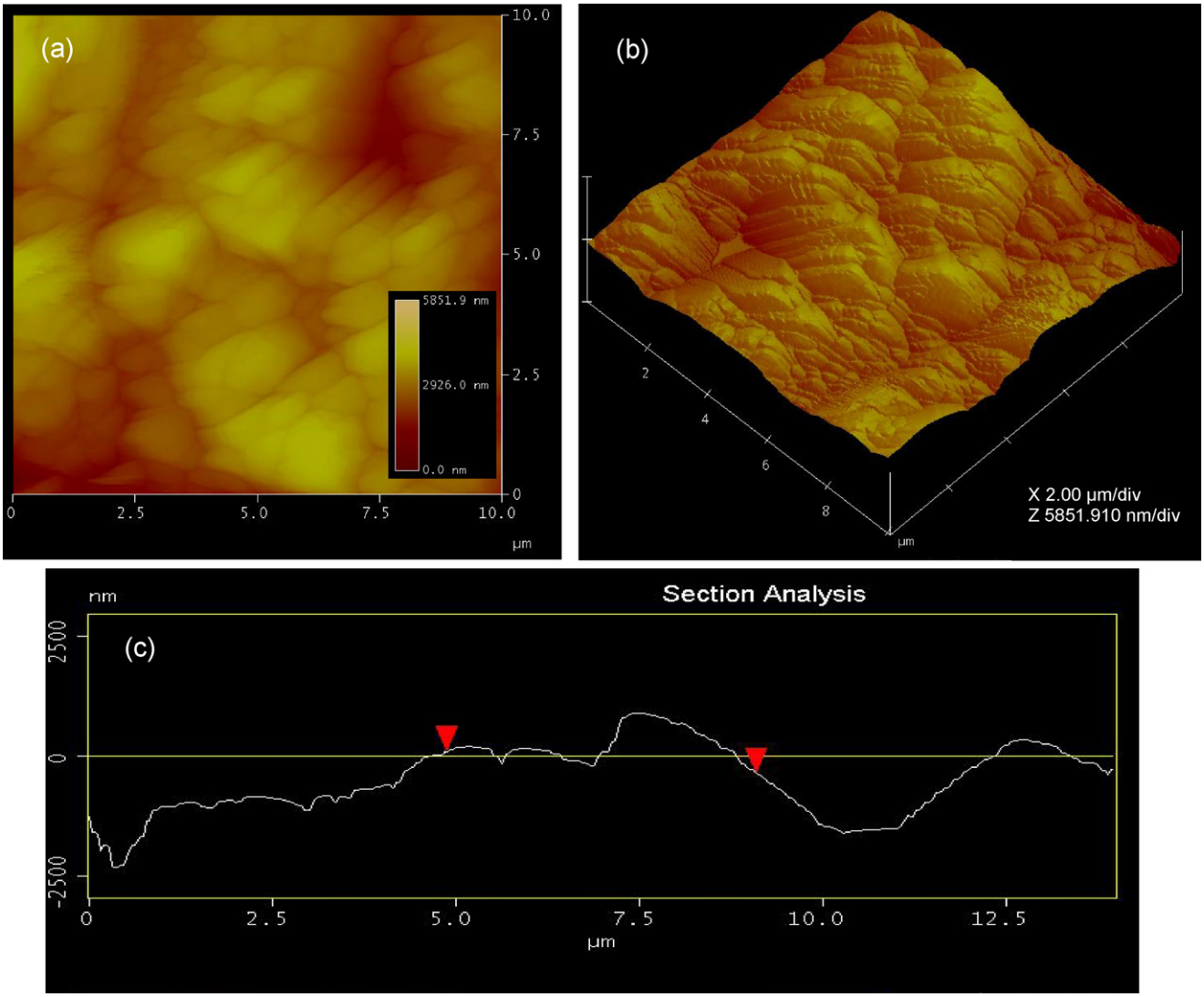

Fig. 5. 2D (a), 3D (b) AFM images, and sectional analysis (c) of Ni-promoted Cd/C catalyst.

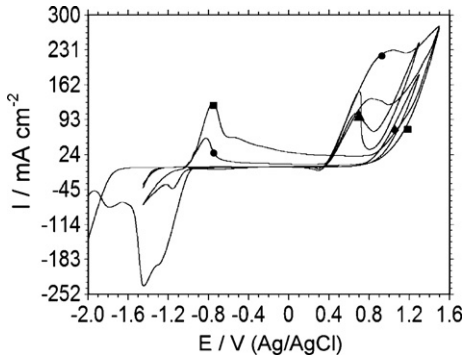

Fig. 6. Cyclic voltammograms of C (♦), Cd/C (■), Ni/C (▲) and Ni-promoted Cd/C (●) in 1.00 M CH_3OH + 1.00 M KOH at 25 °C (scan rate ν: 100 mV s^{-1}).

where it can exert a strong electronic effect [32]. Yu et al. observed an enhancement of formic acid oxidation on the PtBi/C composite electrodes prepared by co-deposition. The oxidation activity changed with electronic effect of the Bi. This attributed to selective blocking of sites at which CO is formed [33].

The electrocatalytic oxidation of methanol occurs not only in the anodic but also continues in the initial stage of the cathodic half cycle. The value of this new oxidation peak which was obtained in the initial stage of the cathodic half cycle was found as 135.2 mA cm^{-2} for Ni-promoted Cd/C. Methanol molecules adsorbed on the surface are oxidized at higher potentials parallel to the oxidation of Ni^{2+} to Ni^{3+} species. The later process has the consequence of decreasing the number of sites for methanol adsorption that along with the poisoning effect of the products or intermediates of the reaction tends to decrease the overall rate of methanol oxidation. Thus, the anodic current passes through a maximum as the potential is anodically swept. In the reverse half cycle, the oxidation continues and its corresponding current goes through a maximum due to the regeneration of active sites for the adsorption of methanol as a consequence of removal of adsorbed intermediates and products. Surely, the rate of methanol oxidation as signified by the anodic current in the cathodic half cycle drops as the unfavorable cathodic potentials are approached.

Fig. 7a shows the effect of the scan rate on methanol oxidation at Ni-promoted Cd/C catalyst in 1.00 M KOH in the presence of 1.00 M methanol. This curve shows that the anodic current for methanol oxidation at Ni-promoted Cd/C catalyst increases rapidly with increasing the potential scan rate and anodic potential shift toward higher potential values (Fig. 7a). Indeed, the time window for methanol oxidation process at higher scan rates becomes very narrow where facile electron transfer takes place between methanol and catalytic sites. The peak currents of the CVs are

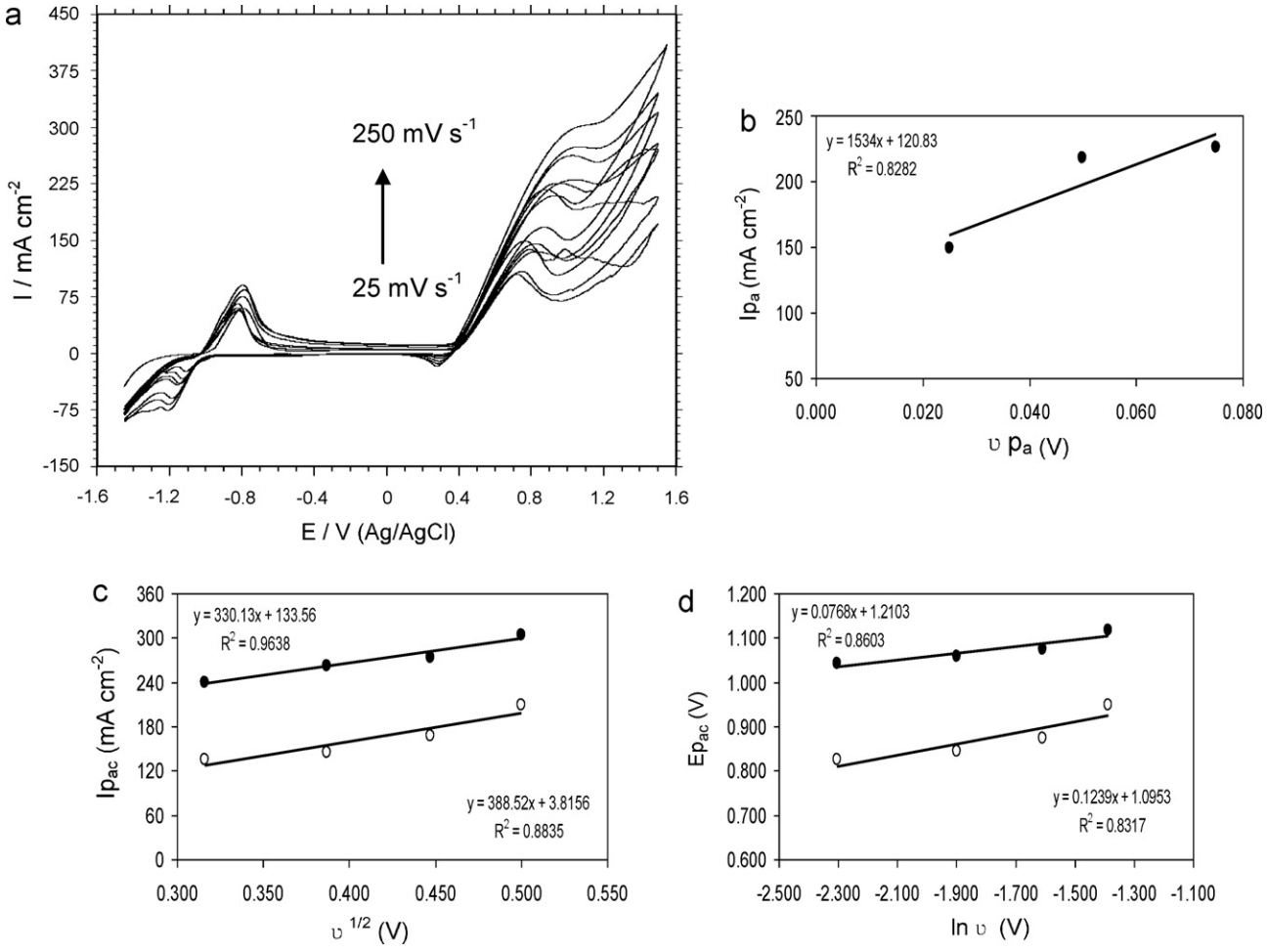

Fig. 7. Effect of the different scan rates (250, 200, 150, 100, 75, 50 and 25 mV s^{-1}) on the electrooxidation of 1.00 M CH_3OH in 1.00 M KOH at the Ni-promoted Cd/C at 25 °C (a). Dependence of anodic peak current during the forward scan on anodic peak potentials (b). Dependence of anodic (●) and cathodic (○) peak current during the forward and reverse scan on the square roots of scan rate (c). Dependence of both anodic (●) and cathodic (○) E_p on ln υ (d).

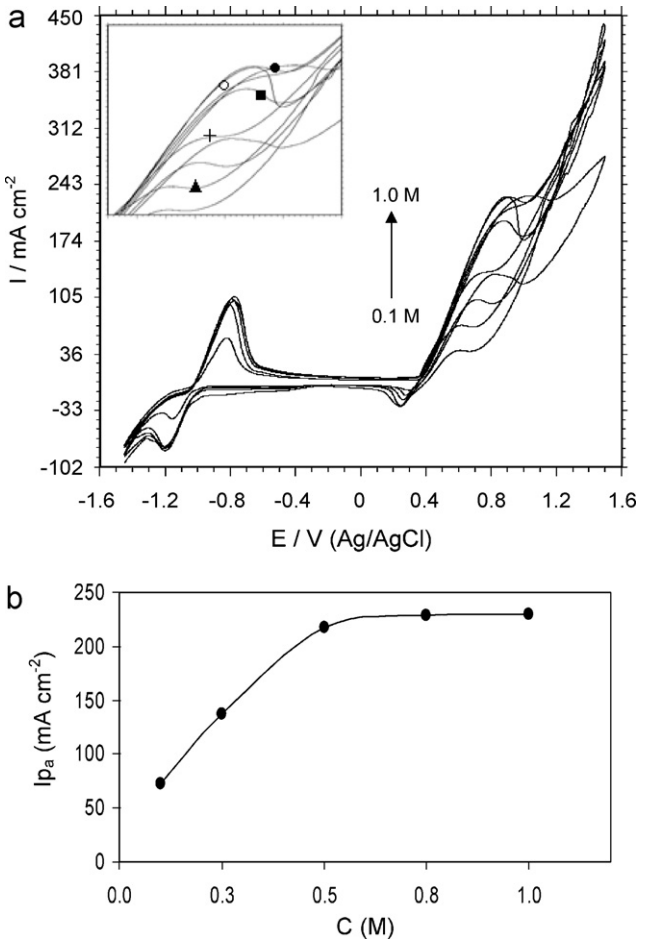

Fig. 8. Effect of the different concentrations of CH_3OH solution ((●) 1.00 M, (○) 0.75 M, (■) 0.50 M, (+) 0.25 M, (▲) 0.10 M) on the electrooxidation of methanol in 1.00 M KOH on the Ni-promoted Cd/C at 25 °C (scan rate ν: 100 mV s^{-1}) (a) (inset shows the zoomed regions of methanol oxidation peaks). C–I_{pa} curve obtained on Ni-promoted Cd/C electrode at 100 mV s^{-1} scan rate (b).

linearly proportional to the scan rate (ν) up to 80 mV s^{-1} (Fig. 7b), from the slope of this line and using [34]

$$I_p = \left(\frac{n^2F^2A\Gamma}{4RT}\right)\nu \quad (1)$$

where I_p, A and Γ are anodic peak current, electrode surface area and surface coverage of the redox species, respectively. The values of Γ were calculated to be approximately 5.76×10^{-6} and 2.34×10^{-6} mol cm^{-2} for Ni-promoted Cd/C and Ni/C catalysts, respectively. In the higher range of υ ($\upsilon > 80$ mV s^{-1}, Fig. 7c), the peak current depends on $\upsilon^{1/2}$, signifying the dominance of a diffusion process as the rate limiting step in the total redox transition of the modifier film. This diffusion process may be due to the charge neutralization of the film during the oxidation/reduction process [35–37]. As it is shown in Fig. 7d, the peak-to-peak separation ($\Delta E_p = E_{pa} - E_{pc}$, $\Delta E_p > 200/n$ mV, n is the number of the exchanged electrons) increases with the scan rate, indicating the limitation arising from charge transfer kinetics. Based on the Laviron theory [38], it is possible to determine the electron transfer coefficient (α) by measuring the variation of the peak potentials with the scan rate (ν) as well as the apparent charge transfer rate constant (k_s) for the electron transfer process between the electrode and the surface-deposited layer according to the following equations:

$$E_{pa} = E^\circ + \frac{RT}{(1-\alpha)nF}\ln\left[\frac{(1-\alpha)Fn\nu}{RTk_s}\right] \quad (2)$$

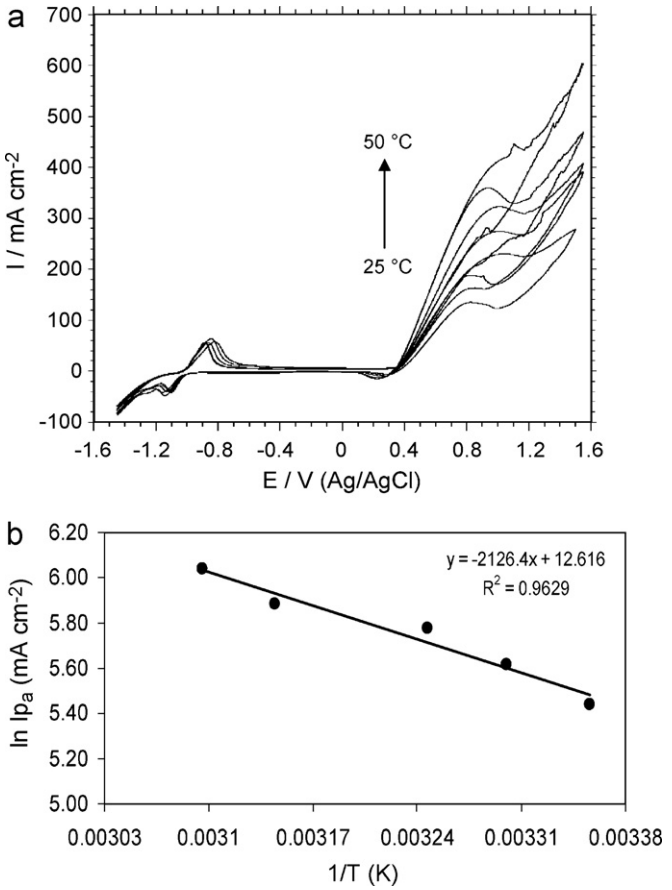

Fig. 9. Effect of the different temperatures on the electrooxidation of methanol in 1.00 M KOH at the Ni-promoted Cd/C (scan rate ν: 100 mV s^{-1}) (a). $1/T$–$\ln I_{pa}$ curve obtained in 1.00 M KOH solution containing 1.00 M methanol on Ni-promoted Cd/C catalyst at 100 mV s^{-1} scan rate (b).

$$E_{pc} = E^\circ + \frac{RT}{\alpha nF}\ln\left[\frac{\alpha Fn\nu}{RTk_s}\right] \quad (3)$$

$$\ln\ k_s = \alpha\ln(1-\alpha) + (1-\alpha)\ln\alpha - \ln\frac{RT}{nF\nu} - \frac{\alpha(1-\alpha)nF\ \Delta E_p}{RT} \quad (4)$$

Fig. 7d shows the plot of E_p with respect to $\ln\upsilon$ from the CVs recorded for Ni-promoted Cd/C catalyst in 1.00 M KOH in the presence of 1.00 M methanol at potential scan rates of 100–250 mV s^{-1} for anodic and cathodic peaks. The anodic electron transfer coefficient (α_a) and cathodic electron transfer coefficient (α_c) were determined as 0.62 and 0.23 and the rate constant, k_s was determined as 0.25 s^{-1} using the plot and Eqs. (2)–(4). This discrepancy between α_a and α_c, suggests that the rate-limiting step for the reduction and oxidation processes might not be the same [39,40]. Since the value of ΔE_p was smaller than 200 mV, α_a and α_c were not calculated for Ni/C.

3.3. Effect of concentration on methanol electrooxidation

Fig. 8 shows the effect of methanol concentration on the anodic peak current at Ni-promoted Cd/C catalyst in 1.00 M KOH. It is clearly observed that as the methanol concentration increases, the peak height increases linearly with methanol concentration up to 0.5 M. It can be assumed that the increase is due to the presence of a diffusion controlled process that appears to play an important role at low methanol concentrations. While the methanol concentration exceeds this limit, the rate of the whole oxidation process seems to be limited by that of the catalytic process in origin, and its

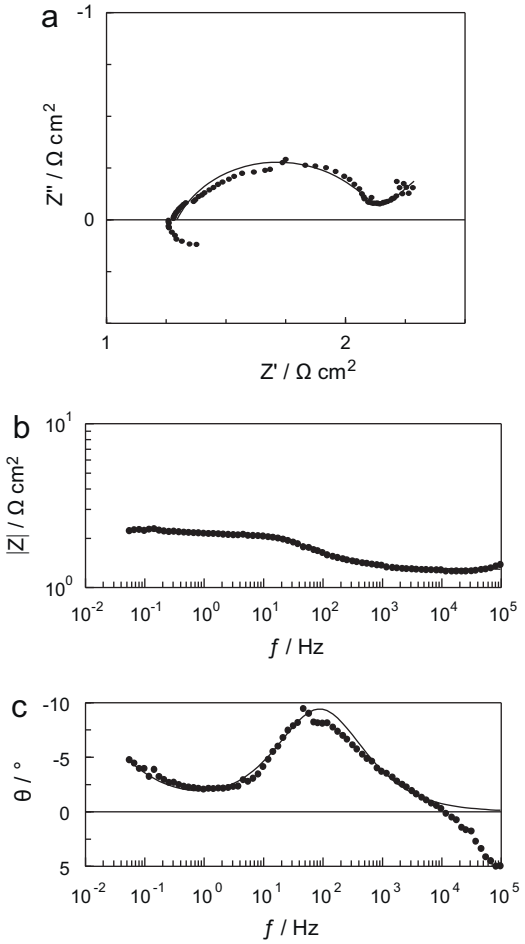

Fig. 10. Nyquist (a), Bode (b) and f–θ (c) plots of Ni-promoted Cd/C at E = 0.50 V vs. Ag/AgCl at 25 °C in 1.00 M CH_3OH + 1.00 M KOH (solid line shows the fitted results).

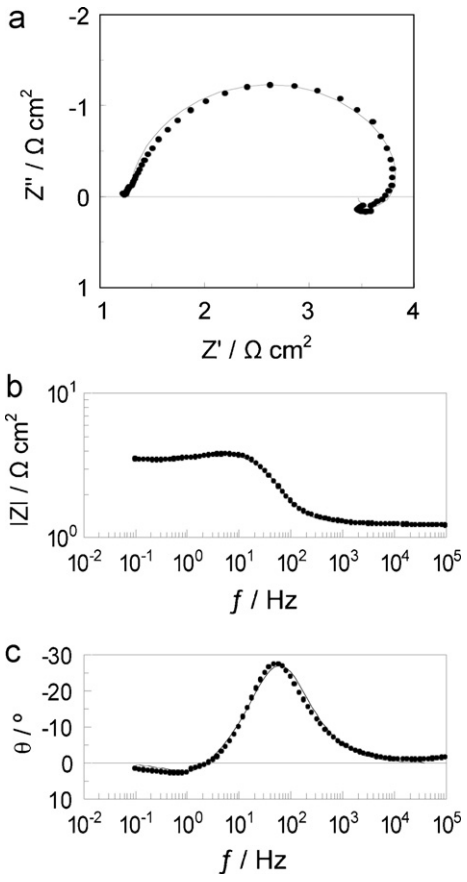

Fig. 11. Nyquist (a), Bode (b) and f–θ (c) plots of Ni/C at E = 0.50 V vs. Ag/AgCl at 25 °C in 1.00 M CH_3OH + 1.00 M KOH (solid line shows the fitted results).

rate depends on the reaction between methanol and Ni^{3+} species, which is present in the film (Fig. 8b).

3.4. Effect of the temperature on methanol electrooxidation

Methanol oxidation on the Ni-promoted Cd/C catalyst in 1.00 M CH_3OH + 1.00 M KOH solution was also performed at different temperatures between 298 and 323 K. The corresponding CVs are shown in Fig. 9a. Methanol oxidation current with rising temperature increased, as expected if the process is thermally activated. However, the potential shift between positive and negative sweeps is not very significant with increasing temperature. Fig. 9b shows the Arrhenius plot for the Ni-promoted Cd/C catalyst, and it is found that almost the regression coefficient is almost close to 1, which means that the relationship between $\ln I_{pa}$ and $1/T$ is good. The apparent activation energy was determined from the slope of the plot of $\ln I_{pa}$ vs. $1/T$ and calculated as 17.69 and 46.25 kJ mol^{-1} for Ni-promoted Cd/C and Ni/C catalysts, respectively. The lower activation energy for the methanol oxidation on Ni-promoted Cd/C catalyst suggests that the Ni-promoted Cd surface structure is beneficial kinetically for the methanol oxidation in alkaline media.

3.5. Electrochemical impedance spectroscopy (EIS) measurements

EIS measurements were performed at 0.5 V potential in order to determine the catalytic activity of prepared catalysts for the methanol oxidation. The representative Nyquist, Bode and f–θ plots for Ni-promoted Cd/C and Ni/C are given in Figs. 10 and 11. As it is seen in Fig. 10, the Nyquist plot of Ni-promoted Cd/C shows a capacitive loop in high frequencies and followed a small straight line in low frequencies. The high frequency capacitive loop is related to the charge transfer resistance (R_{ct}) [41]. The low frequency straight line implies that the methanol oxidation process on Ni-promoted Cd/C catalyst is diffusion controlled [42]. Diameter of the capacitive loop which was observed at the high frequency region was about 0.83 Ω cm^2 and the value of phase angle was −9° (Fig. 10a and c). This was demonstrated that there is a very faster electron-transfer rate on the Ni-promoted Cd/C catalyst. This is not only attributed to the electronic interaction with Ni and Cd on the surface, but may also be caused by the high double-layer capacitance arising from the roughness of the structure of Ni-promoted Cd composite film. For comparison, the curves obtained for Ni/C at 0.5 V potential are also given in Fig. 11. Nyquist's plot of Ni/C catalyst contains two time constants. At the high frequency region, it was observed one capacitive loop and at the low frequency region, appeared inductive loop. This inductive behavior occurs for relaxation phenomena characteristics of the generation of further active sites [43,44] and further adsorption of electroactive constituents, methanol, on active sites [44]. Phase angle was measured as −27° from the curve of f–θ on Ni/C catalyst (Fig. 11c).

The EIS data obtained at 0.5 V potential were fitted by using the electrical equivalent circuit diagrams given in Fig. 12 and the fitting parameters are listed in Table 1. In Fig. 12a, R_{ct} corresponds to charge transfer resistance in Table 1. In this electrical equivalent circuit, R_s, n, CPE and R_{ct} represented the solution resistance, phase shift, a constant phase element and the charge transfer resistance, respectively. In addition, R_{ads} and C_{ads} signify surface adsorption resistance and a capacitance representing the adsorption process. Total polarization resistance was shown

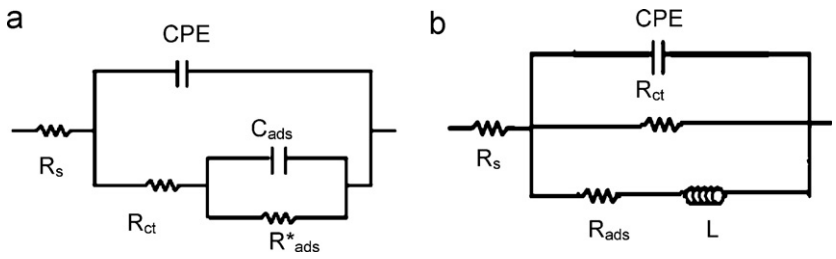

Fig. 12. Electrical equivalent circuit diagram used for modeling electrocatalyst/solution interface in 1.00 M CH_3OH + 1.00 M KOH for Ni-promoted Cd/C (a) and Ni/C (b) catalysts, respectively. $R_p = R_{ct} + R_{ads}$ (R^*_{ads}), R_s: solution resistance; R_{ct}: charge transfer resistance; R^*_{ads}: surface adsorption resistance; R_{ads}: resistance of adsorbated specimen (electroactive constituents, methanol); CPE: double layer capacitance; C_{ads}: related to the adsorption process; L: inductance.

Table 1
The electrochemical data determined from Nyquist plots at 0.5 V potential.

Catalyst	CPE_{dl} ($F\,cm^{-2}$)	n_1	R_{ct} ($\Omega\,cm^2$)	C_{ads} ($F\,cm^{-2}$)	n_2	R_{ads} ($\Omega\,cm^2$)	L (Hz)
Ni/C	0.0026	0.95	2.65			13	1.495
Ni-promoted Cd/C	0.0137	0.75	0.83	7.2	0.55	0.65	

as $R_p = R_{ct} + R_{ads}$. Commonly, the high frequency loop was related to the capacitive character and the low frequency inductive loop was attributed to the relaxation phenomenon characteristics of the generation of further active sites upon the desorption of the intermediates [43–46]. It should be noted that the diffusion process observed during the oxidation process probably would have appeared at very low frequencies with a high or small time constant (Figs. 10 and 11). The low frequency straight line related to the semi-infinite diffusion of the electro-reactant species [42]. The CPE was used in place of a double layer capacitance (C_{dl}) in order to obtain a more accurate fit of the experimental results [47,48]. The CPE value increase in the case of the binary coating was related to the onset of the Faradaic reaction of the methanol oxidation reaction, which indicates the increasing electrocatalytic activity of the catalyst for methanol oxidation [49]. On the other words, the maximum of adsorption capacitance for Ni-promoted Cd/C catalyst fits fairly well with the minimum value of the adsorption resistance parameter. Electrooxidation of the methanol is preceded by the surface adsorption step; consequently, minimum value of the adsorption resistance parameters strongly facilitates the kinetics of the Faradaic electrooxidation process. In addition, this reaction step becomes diffusion-controlled at the peak-current potential (Fig. 10).

It is clear from Table 1 and Fig. 10 that, the charge transfer resistance decreased when a thick Ni-promoted Cd film was electrodeposited on the graphite surface in comparison to that observed at nickel coated graphite catalyst. These results showed that the Ni-promoted Cd/C catalyst has the good electrocatalytic activity for the methanol oxidation. Obtained results from the EIS are in good agreement with the results of the CVs.

3.6. Chronoamperometric measurements

Chronoamperometry (CA) is also used to investigate the electrooxidation of methanol on Ni-promoted Cd/C catalyst. Fig. 13 shows the chronoamperograms obtained at Ni-promoted Cd/C and Ni/C in 1.00 M CH_3OH + 1.00 M KOH solution at E = 0.50 V vs. Ag/AgCl. In Fig. 13, the oxidation current density on the Ni-promoted Cd/C catalyst was increased slowly with time, and then decreased slowly at longer times. This may be caused by the CO-poisoning effect which results in deactivation of the catalyst surface and blocks further oxidation of methanol. There is a sharp decrease in the current density on Ni/C catalyst during the initial stage, followed by a slow decrease over longer periods of time. At the beginning, the active sites are free of adsorbed methanol molecules (fast kinetic rate reaction);

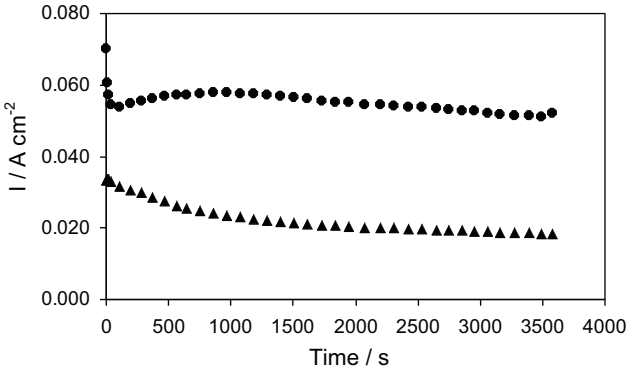

Fig. 13. Chronoamperometric curves recorded in a 1.00 M CH_3OH + 1.00 M KOH solution at E = 0.50 V vs. Ag/AgCl for Ni-promoted Cd/C (●) and Ni/C (▲).

after that, the adsorption of new methanol molecules is a function of the liberation of the active sites by methanol oxidation or intermediate species, such as CO, CH_x and CH_3O formed during the first minutes (rate determining step) [50] that are responsible for poisoning of the catalytic sites. The results imply that the Ni-promoted Cd/C catalyst exhibits higher stability than Ni/C catalyst.

4. Conclusions

Ni-promoted Cd/C catalyst was prepared on the graphite substrate, which was used as the support material for catalysts in the methanol fuel cell applications. Its electrocatalytic activity toward methanol oxidation was evaluated and compared with Ni/C catalyst. The following results can be concluded:

1. The bare graphite and cadmium coated graphite electrodes show no activity for methanol oxidation reaction in 1.00 M KOH.
2. Compact and porous Ni-promoted Cd layer can be successfully prepared on graphite surface.
3. Ni-promoted Cd/C is good catalyst for methanol oxidation reaction, and the highest methanol oxidation current is obtained on this catalyst.
4. CVs at different scan rates, methanol concentrations and temperatures allowed evaluating the methanol oxidation mechanism.
5. Based on the CV, CA, AFM and EIS analyses, Ni-promoted Cd/C catalyst enhanced the electrochemical activity of methanol oxidation because of larger specific surface area, higher surface porosity and synergistic combination.

6. According to the experimental founding, the Ni-promoted Cd catalyst was preferred for use in DMFC.

Acknowledgments

This study has been financially supported by the Çukurova University research fund (Project Number: FEF2010D7). The authors are greatly thankful to Çukurova University research fund.

References

[1] T. Iwasita, Electrochim. Acta 47 (2002) 3663–3674.
[2] N.Y. Hsu, C.C. Chien, K.T. Jeng, Appl. Catal. B: Environ. 84 (2008) 196–203.
[3] J.H. Kim, B. Fang, S.B. Yoon, J.S. Yu, Appl. Catal. B: Environ. 88 (2009) 368–375.
[4] C.S. Chen, F.M. Pan, Appl. Catal. B: Environ. 91 (2009) 663–669.
[5] T.D. Jarvi, S. Sriramulu, E.M. Stuve, J. Phys. Chem. B 101 (1997) 3649–3652.
[6] E. Reddington, A. Sapienza, B. Gurau, R. Viswanathan, S. Sarangapani, E.S. Smotkin, T.E. Mallouk, Science 280 (1998) 1735–1737.
[7] A. Heinzel, V.M. Barragán, J. Power Sources 84 (1999) 70–74.
[8] K. Ramya, K.S. Dhathathreyan, J. Electroanal. Chem. 542 (2003) 109–115.
[9] E. Morallon, A. Rodes, J.L. Vazquez, J.M. Perez, J. Electroanal. Chem. 391 (1995) 149–157.
[10] J.A. Caram, C. Gutierrez, J. Electroanal. Chem. 323 (1992) 213–230.
[11] M. Watanabe, S. Motoo, J. Electroanal. Chem. 60 (1975) 275–283.
[12] T. Yajima, N. Wakabayashi, H. Uiroyuki, M. Watanabe, Chem. Commun. 7 (2003) 828–829.
[13] X.Z. Fu, Y. Liang, S.P. Chen, J.D. Lin, D.W. Liao, Catal. Commun. 10 (2009) 1893–1897.
[14] P.V. Samant, J.B. Fernandes, C.M. Rangel, J.L. Figueiredo, Catal. Today 102 (2005) 173–176.
[15] A. Döner, R. Solmaz, G. Kardaş, Int. J. Hydrogen Energy 36 (2011) 7391–7397.
[16] R. Solmaz, G. Kardaş, Energy Convers. Manage. 48 (2007) 583–591.
[17] I.A. Raj, K.I. Vasu, J. Appl. Electrochem. 20 (1990) 32–38.
[18] R. Solmaz, A. Döner, G. Kardaş, Int. J. Hydrogen Energy 34 (2009) 2089–2094.
[19] S. Berchmans, H. Gomathi, G. Prabhakara Rao, J. Electroanal. Chem. 394 (1995) 267–270.
[20] M. Fleischmann, K. Korinek, D. Pletcher, J. Electroanal. Chem. 31 (1971) 39–49.
[21] M. Uchida, Y. Aoyama, N. Tanabe, N. Yanagihara, N. Eda, A. Ohta, J. Electrochem. Soc. 142 (1995) 2572–2576.
[22] M.A. Abdel Rahim, H.B. Hassan, R.M. Abdel Hameed, Fuel Cells 7 (2007) 298–305.
[23] A.N. Correia, S.A.S. Machado, J. Appl. Electrochem. 33 (2003) 367–372.
[24] Y. Okinaka, in: A.J. Bard, R. Parsons, J. Jordan (Eds.), Standart Potentials in Aqueous Soluion, Marcel Dekker, New York, 1985, p. p. 257.
[25] R. Barnard, J. Appl. Electrochem. 11 (1981) 217.
[26] S.B. Saidman, J.R. Vilche, A.J. Arvia, Electrochim. Acta 32 (1987) 395.
[27] A. Seghiouer, J. Chevalet, A. Barhoun, F. Lantelme, J. Electroanal. Chem. 442 (1998) 113–123.
[28] J.L. Weininger, M.W. Breiter, J. Appl. Electrochem. 110 (1963) 484.
[29] M. Vukovic, J. Appl. Electrochem. 24 (1994) 878–882.
[30] O. Enea, Electrochim. Acta 35 (1990) 375–378.
[31] A.F. Shao, Z.B. Wang, Y.Y. Chu, Z.Z. Jiang, G.P. Yin, Y. Liu, Fuel Cells 10 (3) (2010) 472–477.
[32] L. Ma, X. Zhao, F. Si, et al., Electrochim. Acta 55 (2010) 9105–9112.
[33] X. Yu, P. Pickup, Electrochim. Acta 56 (2011) 4037–4043.
[34] A.J. Bard, L.R. Faulkner, Electrochemical Methods, Fundamentals and Applications, Wiley and Sons, New York, 2001.
[35] M.R. Parra, T. Garca, E. Lorenzo, F. Pariente, Sens. Actuators B 130 (2008) 730–738.
[36] J. Taraszewska, G. Roslonek, J. Electroanal. Chem. 364 (1994) 209–213.
[37] L. Zheng, J.-F. Song, J. Solid State Electrochem. 14 (2010) 43–50.
[38] E. Laviron, J. Electroanal. Chem. 101 (1979) 19.
[39] H. Luo, Z. Shi, N. Li, Z. Gu, Q. Zhuang, Anal. Chem. 73 (2001) 915.
[40] M. Hajjizadeh, A. Jabbari, H. Heli, A.A. Moosavi, A. Shafiee, K. Karimian, Anal. Biochem. 373 (2008) 337–348.
[41] S. Majdi, A. Jabbari, H. Heli, H. Yadegari, A.A. Moosavi-Movahedi, S. Haghgoo, J. Solid State Electrochem. 13 (2009) 407–416.
[42] E. Barsoukov, J.R. Macdonald, Impedance spectroscopy: theory, experiment, and applications, Second Edition, Wiley, New Jersey, 2005.
[43] R.D. Amstrong, M. Henderson, J. Electroanal. Chem. 39 (1972) 81–90.
[44] F. Seland, R. Tunold, D.A. Harrington, Electrochim. Acta 51 (2006) 3827–3840.
[45] S. Majdi, A. Jabbari, H. Heli, A.A. Moosavi-Movahedi, Electrochim. Acta 52 (2007) 4622.
[46] M. Jafarian, M.G. Mahjani, H. Heli, F. Gobal, H. Khajehsharifi, M.H. Hamedi, Electrochim. Acta 48 (2003) 3423–3429.
[47] I. Danaee, M. Jafarian, F. Forouzandeh, F. Gobal, M.G. Mahjani, J. Phys. Chem. B 112 (2008) 15933–15940.
[48] D. Chakraborty, I.B. Chorkendorff, T. Johannessen, J. Power Sources 162 (2006) 1010–1022.
[49] D. Zielinska, B. Pierozynski, J. Electroanal. Chem. 625 (2009) 149–155.
[50] E. Antolini, Appl. Catal. B: Environ. 74 (2007) 337–350.